Reshuffling yeast chromosomes with CRISPR/Cas9

Aubin Fleiss[1], Samuel O'Donnell[1], Téo Fournier[2], Nicolas Agier[1], Stéphane Delmas[1], Joseph Schacherer[2] and Gilles Fischer[1, #]

[1]: Sorbonne Université, CNRS, Institut de Biologie Paris-Seine, Laboratory of Computational and Quantitative Biology, F-75005, Paris, France.

[2]: Université de Strasbourg, CNRS, GMGM UMR7156, Strasbourg, France

[#] corresponding author: Gilles Fischer gilles.fischer@sorbonne-universite.fr

ABSTRACT

Genome engineering is a powerful approach to study how chromosomal architecture impacts phenotypes. However, quantifying the fitness impact of translocations independently from the confounding effect of base substitutions has so far remained challenging. We report a novel application of the CRISPR/Cas9 technology allowing to generate with high efficiency both uniquely targeted and multiple concomitant reciprocal translocations in the yeast genome. Targeted translocations are constructed by inducing two double-strand breaks on different chromosomes and forcing the trans-chromosomal repair through homologous recombination by chimerical donor DNAs. Multiple translocations are generated from the induction of several DSBs in LTR repeated sequences and promoting repair using endogenous uncut LTR copies as template. All engineered translocations are markerless and scarless. Targeted translocations are produced at base pair resolution and can be sequentially generated one after the other. Multiple translocations result in a large diversity of karyotypes including in some instances large segmental duplications. To test the phenotypic impact of translocations, we first recapitulated in a lab strain the *SSU1/ECM34* translocation providing increased sulphite resistance to wine isolates. Surprisingly, the same translocation in a laboratory strain resulted in decreased sulphite resistance. However, adding the repeated sequences that are present in the *SSU1* promoter of the resistant wine strain induced sulphite resistance in the lab strain, yet to a lower level than that of the wine isolate, implying that additional polymorphisms also contribute to the phenotype. These findings illustrate the advantage brought by our technique to untangle the phenotypic impacts of structural variations from confounding effects of base substitutions. Secondly, we showed that strains with multiple translocations display large phenotypic diversity in a wide range of environmental conditions. No coding sequence or promoter region was altered by the multiple translocations showing that simply reconfiguring chromosome architecture is sufficient to provide fitness advantages in stressful growth conditions.

AUTHOR SUMMARY

Chromosomes are highly dynamic objects that often undergo large structural variations such as reciprocal translocations. Such rearrangements can have dramatic functional consequences, as they can disrupt genes, change their regulation or create novel fusion genes at their breakpoints. For instance, 90-95% of patients diagnosed with chronic myeloid leukemia carry the Philadelphia chromosome characterized by a reciprocal translocation between chromosomes 9 and 22. In addition, translocations reorganize the genetic information along chromosomes, which in turn can modify the 3D architecture of the genome and potentially affect its functioning. Quantifying the fitness impact of translocations independently from the confounding effect of base substitutions has so far remained challenging. Here, we report a novel CRISPR/Cas9-based technology allowing to generate with high efficiency and at a base-pair precision either uniquely targeted or multiple reciprocal translocations in yeast, without leaving any marker or scar in the genome. Engineering targeted reciprocal translocations allowed us for the first time to untangle the phenotypic impacts of large chromosomal rearrangements from that of point mutations. In addition, the generation of multiple translocations led to a large reorganization of the genetic information along the chromosomes. Although no gene was disrupted, we showed that solely shuffling the genome resulted in the emergence of fitness advantage in stressful environmental conditions.

INTRODUCTION

Genetic polymorphisms are not restricted to base substitutions and indels but also include large-scale Structural Variations (SVs) of chromosomes. SVs comprise both unbalanced events, often designated as copy number variations (CNVs) including deletions and duplications, and balanced events that are copy number neutral and include inversions and translocations. Both have a phenotypic impact, however the prevalence and the fitness effect of balanced SVs has been less documented than CNVs, partly because they are much more challenging to map than CNVs and also because quantifying their fitness contribution independently from the confounding effect of base substitutions remains challenging. Natural balanced chromosomal rearrangements result from the exchange of DNA ends during the repair of Double Strand Breaks (DSBs) either through Homologous Directed Repair (HDR) between dispersed repeats or intact chromosomes carrying internal repeat sequences homologous to the DNA ends [1,2] or through Non-Homologous End Joining (NHEJ) [3]. Artificial balanced rearrangements are classically engineered by inducing targeted DSBs and promoting repair through both HDR and NHEJ. However, inducing targeted DSBs and engineering scar-less chromosomal rearrangements has remained difficult. In early studies structural variants were obtained through I-SceI-induced DSB repair between split alleles of a selection marker [4,5]. In later developments, the use of the I-SceI endonuclease was combined to a “COunter-selectable REporter” or CORE cassette in the frame of the *delitto-perfetto* technique, allowing the generation of a reciprocal translocation in a scar-less fashion [6]. Other techniques based on Cre/Lox recombination were used to make the genomes of *Saccharomyces cerevisiae* and *Saccharomyces mikatae* colinear and generated interspecific hybrids that produced a large proportion of viable but extensively aneuploid spores [7]. Cre/Lox recombination was also used to assess the impact of balanced rearrangements in vegetative growth and meiotic viability [8–10]. A novel approach using yeast strains with synthetic chromosomes allowed extensive genome reorganization through CreLox-mediated chromosome scrambling [11–14]. This approach proved to be efficient to generate strains with a wide variety of improved metabolic capacities [13,15–17]. Muramoto and collaborators recently developed a genome restructuring technology relying on a temperature-dependent endonuclease to conditionally introduce multiple rearrangements in the genome of *Arabidopsis thaliana* and *S. cerevisiae,* thus generating strains with marked phenotypes

such as increased plant biomass or ethanol production from xylose [18]. Methods using Zinc Finger Nucleases (ZFNs) and Transcription Activator-Like Effector Nucleases (TALENs) were also developed to generate targeted rearrangement in yeast, mammalian and zebrafish cells [19–22]. Although these technologies provide very useful insights, they are often difficult to implement and/or rely on the use of genetic markers. For this reason, the development of the CRISPR/Cas9 (Clustered Regularly Interspaced Short Palindromic Repeats/CRISPR associated) system has boosted the field of genome engineering [23–25]. This system, initially derived from immune systems of bacteria, consists of an endonuclease encoded by the Cas9 gene of *Streptococcus pyogenes* and a short RNA that guides the endonuclease at the targeted genomic locus. The gRNA can be easily designed to target any genomic locus proximal to a “NGG” Promoter Adjacent Motif (PAM). This technology is now routinely used to introduce targeted DSBs in genomes from a wide variety of species [26]. In yeast, CRISPR/Cas9 induced DSBs can be repaired with high efficiency by providing homologous repair DNA cassettes, allowing a variety of genome editions. Previous studies achieved the introduction of point mutations, single and multiple gene deletions and multiplexed genome modifications at different loci by transforming cells with plasmids bearing single or multiple gRNAs and linear DNA repair templates [27–30]. CRISPR-based approaches have also been developed to add centromeres and telomeres to chromosome fragments [31] concatenating chromosomes [32,33] and for massively parallel genome editing to generate large libraries of genetic variants [34–36]. Interestingly, it has been noticed that multiplex genome editing can often result in undesirable chromosomal translocation suggesting that such rearrangements are likely programmable [37]. The ability to generate genome rearrangements with CRISPR/Cas9 has been known for some time [38] and more recently used to engineer translocations in mammalian cells with high efficiency. The principle was to introduce two DSB in two distinct chromosome with CRISPR, then repair the DNA ends in trans by HDR with donor DNA carrying a selection marker, lost in a second step by Cre/Lox recombination leaving a single loxP element at the chromosomal junction [39]. However, unequivocally determining the contribution of SVs to phenotype variations in a large variety of environmental conditions and independently from the contribution of single nucleotide variants cannot be envisioned in mammals because of overwhelming technical and ethical difficulties.

In this study, we developed two CRISPR-Cas9 genome editing strategies in yeast to generate markerless and scarless SVs with high efficiency in a control and unique genetic background, thus providing a mean to quantify their fitness impacts by high-throughput phenotyping independently from marker or background specific effects. The first strategy allowed generating on-demand any translocation at a base-pair resolution and we recapitulated the phenotypic consequences associated with known rearrangements. The second approach allows generating multiple SVs simultaneously leading to an important diversity of karyotypes. We showed that reshuffling the chromosome architecture between dispersed repeated sequences without disrupting any genes or changing their promoter sequences is sufficient to create fitness diversity in various stress conditions.

134 **RESULTS**

135 **Rationale for chromosome reshuffling**

136 We used a single-vector which encodes both the Cas9 nuclease gene and a gRNA expression
137 cassette. This cassette allows cloning either a DNA fragment of 430 base-pairs reconstituting two
138 different gRNAs in tandem or a unique 20 bp fragment corresponding to the target sequence of a
139 single gRNA (fig 1A). This system is versatile as it allows generating either a single targeted or
140 multiple translocations at once. Targeted translocations can be induced by a pair of gRNAs
141 generating two concomitant DSBs in two different chromosomes. Any pair of gRNAs can be cloned
142 in the vector in a single ligation step using as insert either a synthetic DNA fragment or a PCR
143 product (see Methods). The two DSBs are repaired in trans upon homologous recombination with
144 chimerical donor DNA resulting in targeted reciprocal translocations with a single-nucleotide
145 precision (fig 1B). Multiple translocations are induced by generating several DSBs using a single
146 gRNA that targets repeated sequences such as the Long Terminal Repeats (LTRs) scattered on
147 different chromosomes. The multiple DSBs are repaired by recombination using the uncut copies
148 of the LTRs as homologous templates (fig 1C). Both targeted and multiple translocations are
149 engineered in a scar-less fashion and without integrating any genetic marker in the genome.

150

Figure 1

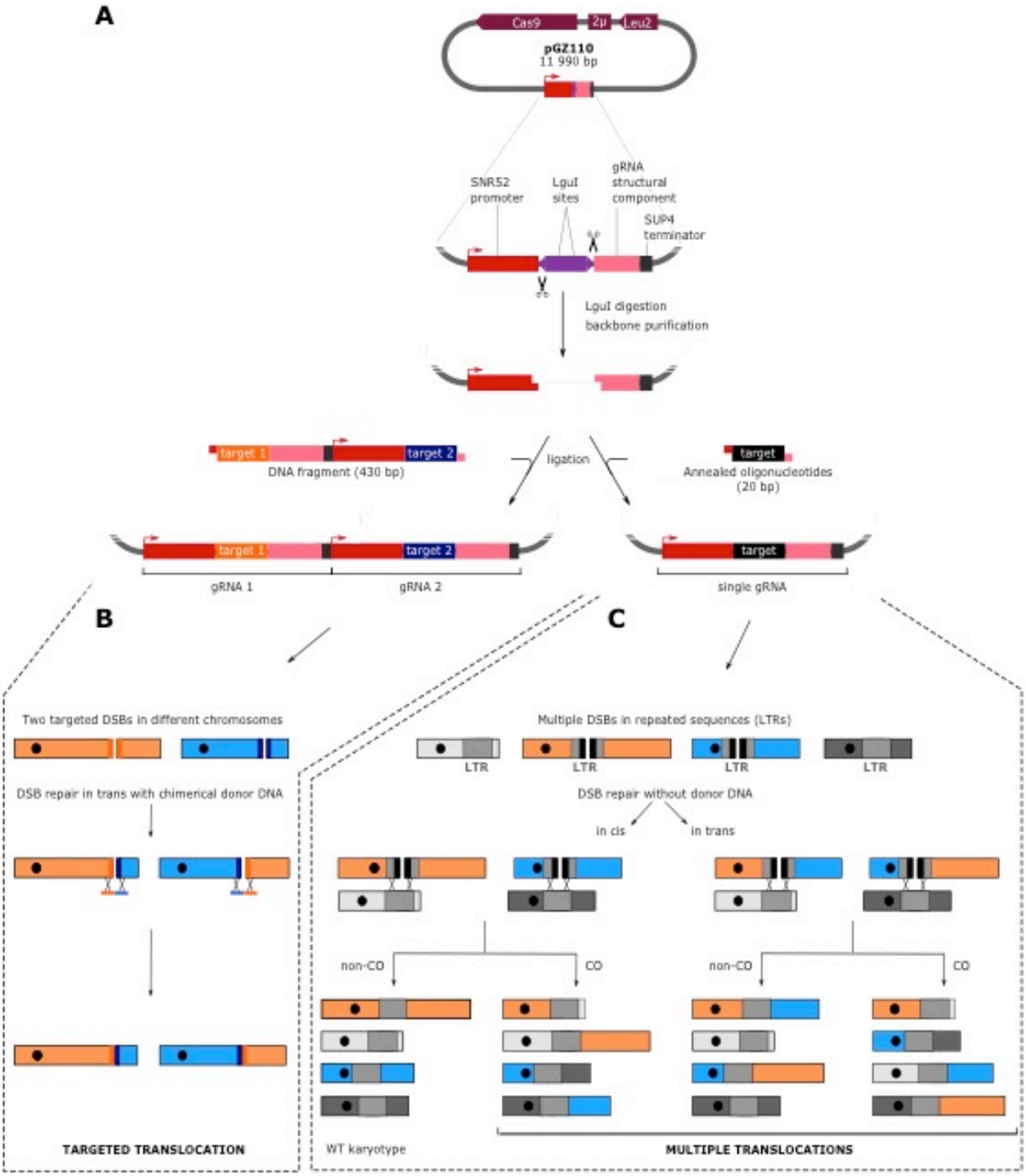

Figure 1:Strategy to reshuffle the yeast genome. A. Cloning gRNA target sequences in the pGZ110 vector (Bruce Futcher, Stony Brook University). Upon digestion, the two LguI sites generate non-complementary single strand overhangs of 3 bases. This system is versatile as it allows to clone in a single ligation step either a DNA fragment of 430 base-pairs reconstituting two different gRNA expression cassettes in tandem (left) or a 20 bp oligonucleotide corresponding to the target sequence of a unique gRNA (right). **B.** Induction of a targeted reciprocal translocation. Two DSBs are induced in different chromosomes and are repaired by homologous recombination with chimerical donor DNA oligonucleotides. The bold lines flanking the DSBs symbolize the target sequences. Donor DNAs force the repair to occur

159 in trans (i.e. between two ends coming from the two different DSBs). **C.** Induction of multiple reciprocal translocations.
160 This example illustrates a situation where the only two LTRs located in the blue and orange chromosomes are targeted
161 by the gRNA (bold black lines indicate the target sequences) while LTRs located in the two grey chromosomes are not
162 cut (devoid of target sequence). Note that more LTRs can be targeted as detailed below (see fig 5). DSBs are repaired
163 by homologous recombination using the uncut LTRs as donor template. Repair can occur in cis (i.e. the two ends from
164 the same DSB are repaired together) or in trans (i.e. two ends from two different DSBs are repaired together).

165 **Engineering a markerless reciprocal translocation at single base-pair resolution**

166 We first engineered a reciprocal translocation between two reporter genes leading to phenotypes
167 easy to observe upon disruption. Mutation in the *ADE2* gene involved in purine nucleotide
168 biosynthesis results in the accumulation of a red pigment while mutating the *CAN1* gene which
169 encodes an arginine permease confers canavanine resistance to the cells. To generate two
170 concomitant DSBs on chromosomes V and XV carrying *CAN1* and *ADE2*, respectively, we cloned
171 two previously described gRNA target sequences, namely CAN1.Y and ADE2.Y [27]. To repair the
172 DSBs, we used donor DNA fragments of 90 base-pairs each composed of two homology regions of
173 45 bp identical to the sequences flanking CRISPR cutting sites (supp table 1). Two combinations of
174 DNA repair donor fragments were used. As a control, we used donors called Point Mutation-donors
175 (PM-donors), promoting the intra-chromosomal repair of DSBs in cis and mutating PAM sequences
176 into stop codons, thus preventing further Cas9 activity. The donors promoting inter-chromosomal
177 repair in trans, thus leading to a Reciprocal Translocation were called RT-donors. No point
178 mutation needed to be introduced into the PAM sequence in this case because the translocation
179 generates chimerical target sequences not complementary to the original gRNAs (fig 2A).
180 Transformation with the plasmid bearing two gRNAs and either RT or PM-donors resulted in 95%
181 and 76% of the colonies showing both the pink and resistance to canavanine phenotypes [ade2,
182 can1], respectively (Material and Methods, fig 2B). In the RT-donor experiment the other 5% of
183 colonies were all white and sensitive to canavanine, probably resulting from the transformation of
184 the *LEU2* marker without induction of any DSB. In the PM experiment, we recovered 21% of white
185 colonies, 83% of which being resistant to canavanine, likely resulting from a single DSB/repair in
186 the *CAN1* gene. We also recovered 3% of pink and sensitive colonies likely resulting from a single
187 DSB/repair in the *ADE2* gene (fig 2B). We then confirmed by PCR the presence of the chimerical
188 chromosomal junctions of 16 [ade2, can1] strains recovered from the RT experiment. We further

189 validated the translocation by karyotyping two [ade2, can1] strains by PFGE. No other visible
190 chromosomal rearrangements could be observed apart from the expected translocated
191 chromosomes VtXV and XVtV (fig 2C). Sanger sequencing of 250 bp around the chimerical
192 junctions of these two strains confirmed that the translocation occurred right at the position defined
193 by the sequence of the RT-donors with no additional mutations (supp fig 1).

Figure 2

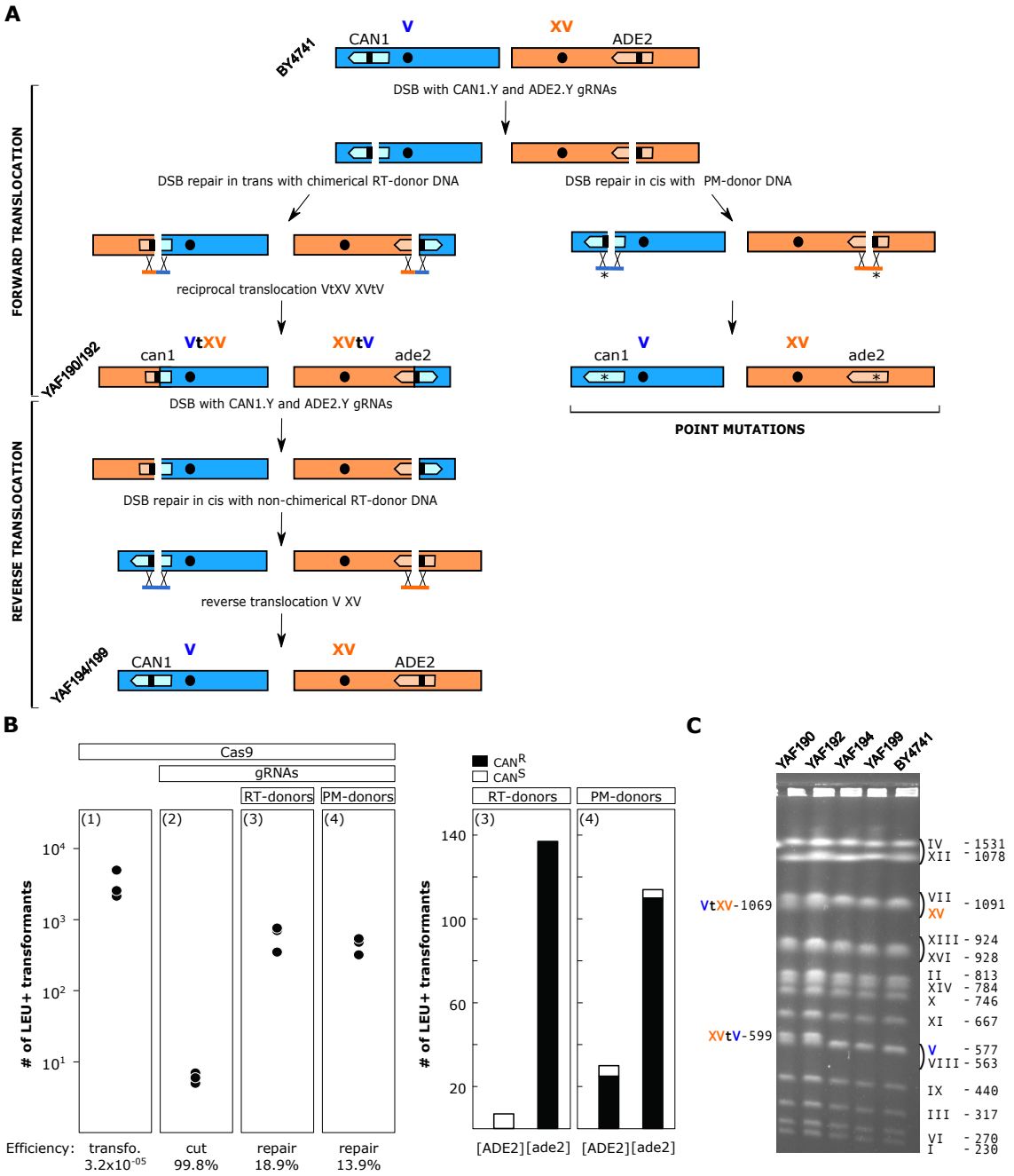

194

195 **Figure 2: A Reversible markerless translocation. A.** PAM sequences are symbolized by the small black bars within
196 the *CAN1* and *ADE2* genes in dark blue and orange. RT- and PM-donors stand for Reciprocal Translocation and Point
197 Mutation donor DNAs used to repair the DSBs. The point mutation responsible for the introduction of the STOP codon in

198 the PAM sequence is indicated by an asterisk. Strain names are written in diagonal. **B.** Left: plots indicating the number
199 of transformants for 10^8 transformed cells obtained in 3 independent experiments. Panels (1) and (2) illustrate the
200 efficiency of transformation with the Cas9 plasmid and cutting efficiency of the gRNAs, respectively. Panels (3) and (4)
201 show DSB repair efficiency at the *ADE2* and *CAN1* loci by both the Reciprocal Translocation (RT) and Point Mutation
202 (PM) donor DNAs (Methods). Right: Histograms of the numbers of white [ADE2], pink [ade2], canavanine resistant
203 [CAN^R] and sensitive [CAN^S] colonies obtained with the RT (3) and PM donors (4), 100% and 96% of [ade2]
204 transformants are also mutated for the *CAN1* gene, respectively. **C.** PFGE karyotypes of two strains carrying the *ADE2-*
205 *CAN1* translocation (YAF190, YAF192) and two strains with the reverse translocations restoring the original
206 chromosomes V and XV (YAF194 and YAF199 originating from YAF190 and YAF192, respectively). Chimerical
207 chromosomes are denoted VtXV and XVtV. Original chromosome XV and V from the reference strain BY4741 are
208 indicated in orange and blue respectively. Chromosome size is indicated in kb.

209 We next showed that our system allows to sequentially generate several targeted translocations.
210 To illustrate this we performed the reverse translocation to restore the WT chromosomes V and XV
211 and functional *ADE2* and *CAN1* genes in the strains that carried the *ADE2-CAN1* translocation
212 (YAF190 and YAF192 in fig 2C). We took advantage of the high instability of the Cas9 plasmid that
213 can be easily cured from the strains (Material and Methods). We first cured the plasmid from the
214 two translocated strains. Then, we cloned a pair of gRNAs that target the chimerical junctions
215 formed by the *ADE2-CAN1* translocation in the Cas9 plasmid and designed repair donors to
216 restore *ADE2* and *CAN1* to their original configuration (fig 2A, supp table 1). Co-transformation
217 with the gRNAs plasmid and donor fragments resulted in 94.2% of colonies which restored the
218 white and canavanine sensitive phenotypes [ADE2, CAN1]. We performed pulse field gel
219 electrophoresis (PFGE) karyotyping of two [ADE2, CAN1] strains. No difference could be observed
220 between the karyotype of these two strains and that of the original BY4741 strain (YAF194 and
221 YAF199 in fig 2C). The chromosomal junctions of the two de-translocated strains were Sanger-
222 sequenced and were found identical to BY4741 natural junctions (supp fig 1). These results
223 demonstrate that sequential chromosomal translocations can be engineered at base-pair resolution
224 with high efficiency.

225 Finally, we also showed that our system can be used to simultaneously generate a deletion of a few
226 nucleotides and a reciprocal translocation. We used the same CAN1.Y and ADE2.Y gRNA target
227 sequences as above and designed new donor fragments inducing deletions of 27 and 23 bp,
228 including the PAM sequences, on chromosome V and XV, respectively (supp fig 2A, supp table 1).

229 As above, we obtained a high proportion of [*ade2*, *can1*] transformants (96%). PCR of the junctions
230 and karyotyping of 4 strains showed that chromosome V and XV underwent the expected
231 reciprocal translocation (fig 3 A). The genome of one translocated strain was Nanopore sequenced
232 and *de-novo* assembled (Material and Methods, supp table 2 and 3) to check whether off-target
233 activity of the Cas 9 nuclease could result in unexpected additional rearrangements. The
234 translocated and reference genomes were entirely collinear except for the expected translocation
235 and associated deletions on chromosomes V and XV (fig. 3B). No other rearrangement was
236 observed, suggesting no major off-target activity of the Cas9 nuclease in this strain. In addition, the
237 junction sequences are identical to the sequences of the chimerical donor fragments (supp fig 2B).
238 These experiments demonstrate that a deletion and reciprocal translocation can be concomitantly
239 engineered at base-pair resolution with CRISPR/Cas9 in the yeast genome.

Figure 3

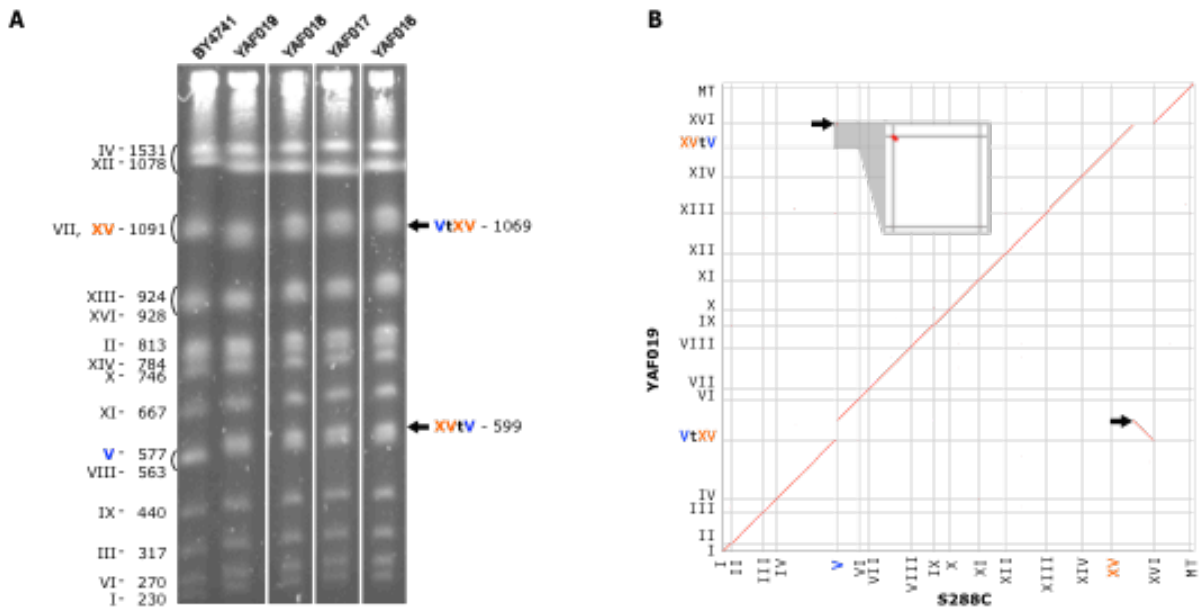

240

241 **Figure 3: A non-reversible translocation between *ADE2* and *CAN1* genes**. (A) PFGE karyotypes of 4
242 independent strains carrying the translocation (YAF016 to YAF019). All symbols are identical to Fig. 2C. (B)
243 Homology matrix of *de-novo* assembled strain YAF019 vs S288c reference genome. Translocated fragments
244 are indicated by black arrows.

245 **Recapitulating a natural translocation involved in sulphite resistance in wine strains**

246 It was previously reported that a reciprocal translocation between the promoters of *ECM34* and
247 *SSU1*, a sulphite resistance gene, created a chimerical *SSU1-R* allele with enhanced expression

248 resulting in increased resistance to sulphite in the wine strain Y9J [40]. This translocation resulted
249 from a recombination event between 4 base-pair micro-homology regions on chromosomes VIII
250 and XVI. We therefore engineered the same translocation into the BY4741 background. We
251 designed two gRNA target sequences as close as possible to the micro-homology regions (supp
252 fig 3A and supp table 1). The first gRNA targeted the *SSU1* promoter region, 115 base-pairs
253 upstream of the start codon. The second gRNA targeted the promoter region of *ECM34*, 24 base-
254 pairs upstream of the start codon. To mimic the translocated junctions present in the wine strains,
255 we designed 2 double stranded synthetic DNA donors of 90 base-pairs centered on the micro-
256 homology regions but not on the cutting sites. In addition, each donor also contained a point
257 mutation in the PAM sequences to prevent subsequent CRISPR recognition (supp fig 3A).
258 The transformations with the Cas9 plasmid containing the two gRNAs and the donor DNA yielded
259 on average 202 transformants. We tested natural and chimerical junction by colony PCR for 16
260 transformants and found the expected chimerical junctions in 15 of them. This translocation was
261 not visible by PFGE karyotyping because the size of the translocated chromosomes were too close
262 to the size of the original chromosomes (XVI 948 kb, VIII 563 kb, VIIItXVI 921 kb and XVItVIII 599
263 kb). To further validate the rearrangement, we checked the junctions by southern blot for one
264 translocated strain with probes flanking the two cutting sites on chromosome VIII and XVI (supp fig
265 3B). This experiment validates the presence of the chimerical junction fragments in the rearranged
266 strain YAF082 as compared to the WT. Finally, we sequenced the junctions of the translocated
267 strain and found that the rearrangement occurred within the expected micro-homology regions
268 (supp fig 3C). In addition, the system was designed such that both mutated PAMs ended up into
269 the promoter of *ECM34* the translocation, therefore unlikely to have any impact on the expression
270 of the sulphite resistance gene *SSU1* (supp fig 3C).
271 We then compared sulphite resistance between the lab strain in which we engineered the
272 translocation (YAF202 corresponding to YAF082 cured for the Cas9 plasmid, see Methods), the
273 non-translocated parental lab strain (BY4741) and wine isolates that carry or not the translocation
274 of interest (Y9J and DBVPG6765, respectively). Surprisingly, we found that the engineered strain
275 with the translocation was the least resistant of all strains with a Minimal Inhibitory Concentration
276 (MIC) of 1 mM (fig. 4). By comparison, the reference strain and the wine isolate without the

277 translocation both had a MIC of 2 mM. This suggests that the promoter of *ECM34* is weaker than
278 the *SSU1* promoter in the BY background. As expected, the wine isolate with the translocation
279 (Y9J) was the most resistant of all (MIC > 20 mM, fig. 4), However, it was reported that this wine
280 strain also had four tandem repeats of a 76 bp segment in the promoter region of *SSU1* originating
281 from the *ECM34* locus and it was shown that the number of repeats positively correlated with
282 sulphite resistance [40]. This suggested that the translocation would not be *per se* responsible for
283 increased resistance. Resistance would in fact result from the repeats in the *ECM34* promoter
284 region that were brought in front of the *SSU1* gene by the translocation. There is only one copy of
285 this 76 bp sequence in the BY background. To test whether promoter repeats were responsible for
286 the resistance phenotype we PCR amplified the repeat-containing promoter of the translocated
287 wine strain Y9J (introducing a point mutation in the PAM sequences to avoid subsequent
288 recognition by Cas9, supp table 1) and used the PCR product as donor in a CRISPR experiment to
289 introduce the promoter repeats in front of the *SSU1* gene in the translocated BY4741 strain. We
290 designed a gRNA targeting the region between the single copy motif and the beginning of *SSU1*
291 (supp table 1). We obtained hundreds of transformants and found that 5 out of 8 transformants
292 tested by PCR contained the four tandem repeats and were subsequently validated by Sanger
293 sequencing (supp fig 3D). The addition of the repeats in the *SSU1* promoter in the translocated lab
294 strain (YAF158) resulted in increased sulphite resistance with a MIC of 7 mM (fig. 4) therefore
295 confirming the effect of the repeats on the resistance phenotype. However, the chromosomal
296 configuration and the promoter repeats are the same in YAF158 and the Y9J wine strain, yet the
297 wine strain is much more resistant than the lab strain suggesting that additional polymorphisms
298 must contribute to the phenotype in the wine isolate.

Figure 4

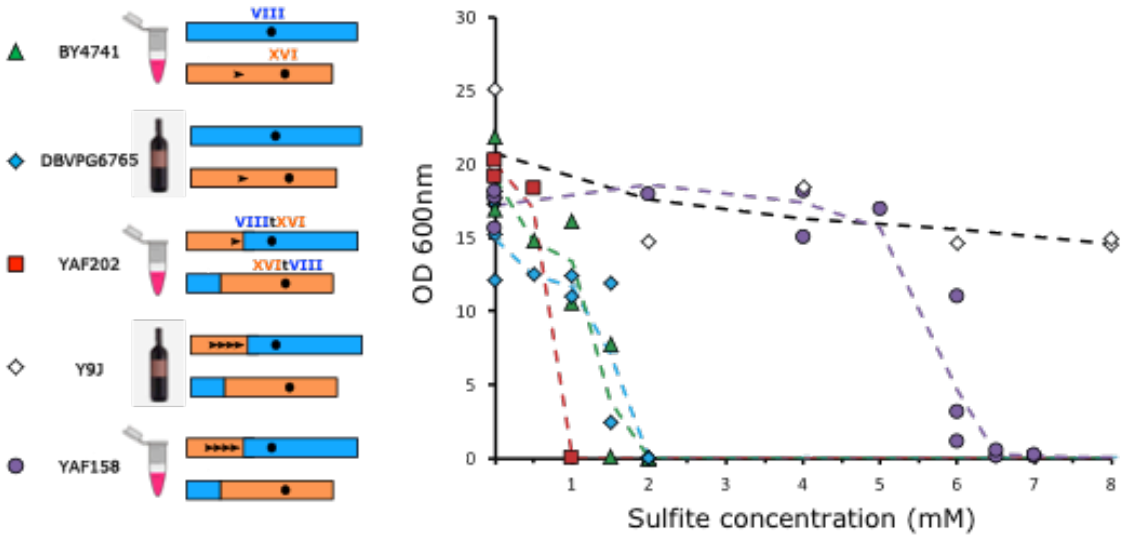

299

300 **Figure 4: Quantification of sulphite resistance.** Laboratory and wine strains are symbolized by eppendorf
301 tubes and bottles, respectively. The chromosomal configurations are represented by blue and orange
302 rectangles. Black arrowheads symbolize the 76 bp repeats in promoter regions. The determination of the
303 MIC of sulphite was performed for the entire range of concentration for all strains but for readability all points
304 with a null value of OD for concentrations higher than the MIC were omitted from the graph.

305 **Reshuffling chromosomes with multiple translocations**

306 It has been previously shown that DSBs give rise to chromosomal rearrangements when they fall
307 in dispersed repetitive elements such as Ty retrotransposons [1]. We reasoned that generating in a
308 single step multiple DSBs targeting Ty repeated sequences should also result in genome
309 reshuffling through multiple translocations without altering any coding sequence or promoter region.
310 We chose a gRNA sequence flanked by a PAM that targets 5 different Ty3 LTR copies located in
311 chromosomes IV, VII, XV and XVI (four of which comprise a region identical to the gRNA target
312 sequence while the fifth copy differs from the target sequence by a single mismatch at its 5' end,
313 fig 5A). In addition, there are 30 other complete copies of Ty3 LTRs dispersed throughout the
314 genome but they contain several mismatches or indels relatively to the sequence of the gRNA
315 and/or are devoid of PAM, suggesting that Cas9 will not cut at these sites (fig 5A). We
316 hypothesized that these uncut LTRs would be used as internal donor templates for DSB repair. We
317 chose to target these five Ty3 LTRs because inducing DSB at these locations should allow

318 significant genome reshuffling without compromising to much the viability of the cells by
319 overloading the repair system by too many DSBs. DNA ends originating from the five DSBs can be
320 repaired both in cis, *i.e.* the two ends from the same DSB are repaired together or in trans, *i.e.* the
321 two ends from two different DSBs are repaired together. A WT-like karyotype is expected when all
322 DSBs are repaired in cis and without any crossover with the internal Ty3 donor templates (type A
323 in fig 5B). In addition, we can predict 23 viable combinations of rearranged karyotypes when all
324 DSBs are repaired in trans without crossover (types B to X in fig 5B). Note that only reciprocal
325 translocations are expected because the two targeted Ty3 LTRs on chromosome XV are in the
326 same transcriptional orientation and therefore cannot induce the inversion of the intervening
327 segment. In addition, all rearranged karyotypes comprising acentric or dicentric chromosomes are
328 supposedly non-viable and thus will not be recovered. Other combinations of viable karyotypes
329 resulting from both cis and trans repair with crossovers within uncut LTR donors could also be
330 generated but are hard to predict because of the large number of possible LTR donors that can be
331 used as template for repair and therefore are classified as 'unpredicted' in the following.
332 We transformed BY4741 and BY4742 cells with the Cas9/gRNA plasmid targeting the 5 Ty3 LTRs
333 and recovered a total of 211 and 159 transformants, respectively. We PFGE karyotyped 69
334 transformants (37 BY4741 and 32 BY4742) out of which 30 showed clear chromosomal
335 rearrangements on the gels, representing 18 different karyotypes in total (fig 5C). This result
336 demonstrates that genomes are efficiently reshuffled via our strategy. In total 23 strains showed
337 predicted rearrangements, representing 10 distinguishable profiles (B; D; (F,M,T); G; H; J; (K,N); R;
338 V and X in fig 5B and 5C). We validated the presence of most predicted junctions by colony-PCR
339 in 18 out of the 23 strains (fig 5C). We sequenced all chromosomal junctions in 2 strains that show
340 the most frequently observed rearranged profile (type J in fig 5B and 5C) and found that all
341 junctions, from both chimerical and un-rearranged chromosomes, were mutated in their PAM
342 compared to the original target sequence (supp fig 4). This shows that during shuffling, all targeted
343 sites were cut and repaired using as donor uncut Ty3 LTRs that had no PAM. Additional mutations
344 in the region corresponding to the gRNA target sequence were also observed for 3 junctions, but
345 were too few to identify which copy of the uncut Ty3 LTR was used as donor (supp fig 4). We
346 tested any possible over- or under-representation of the predicted rearranged types by randomly

347 sampling with replacement 15 draws (corresponding to the 15 characterized strains) in a uniform
348 distribution of 18 types (24 types excluding type A (not rearranged) and types (F,M,T) and (K,N)
349 that are not discernible). We performed 10,000 realizations and counted the number of times we
350 sampled the different types. The probability to observe 5 times the predicted type J was 0.017
351 which suggests that this type could be overrepresented. No other type showed deviation from
352 expectation. However, given the relatively small number of characterized strains, we cannot
353 exclude that DSBs would be repaired in a random way.
354 Moreover, we obtained 7 strains with distinct unpredicted karyotypes involving chromosomes other
355 than the 4 targeted ones (fig 5C). For instance, chromosomes XI and XIV that have no PAM
356 sequence associated with their Ty3 LTRs (fig 5A) are absent from several karyotypes showing that
357 they can be rearranged in the absence of DSB (fig 5C). Surprisingly, some of karyotypes showed
358 an apparent genome size increase suggesting the presence of unexpected large duplications (see
359 YAF064, YAF126, YAF143 and YAF150 in fig 5C). Using Oxford Nanopore MinION, we sequenced
360 and *de-novo* assembled the genome of YAF064. We characterized in this strain an unequal
361 reciprocal translocation between chromosomes VII and XV (supp fig 5A). The junctions
362 corresponded to the targeted CRISPR cut site on chromosome XV but not on chromosome VII. In
363 the chimerical chromosome XVtVII, the junction occurred away from the expected site resulting in
364 a 30 kb increase in DNA content. In the chimerical chromosome VIItXV, the junction also occurred
365 away from the expected site but was accompanied by a truncated triplication of a 110 kb region.
366 The missing part of the triplication corresponds to the 30 kb region found in the reciprocal
367 chromosome XVtVII. The sequencing coverage relatively to the reference genome clearly
368 confirmed the triplication of the complete 110 kb region (supp fig 5B). Interestingly the 110 kb
369 segment, composed of regions *a* and *b*, is flanked by two Ty3 LTRs. Moreover, two full length Ty2
370 retrotransposons are found, one in chromosome XV directly flanking the targeted Ty3 LTR and the
371 other one in chromosome VII at the junction between regions *a* and *b* (supp fig 5C).

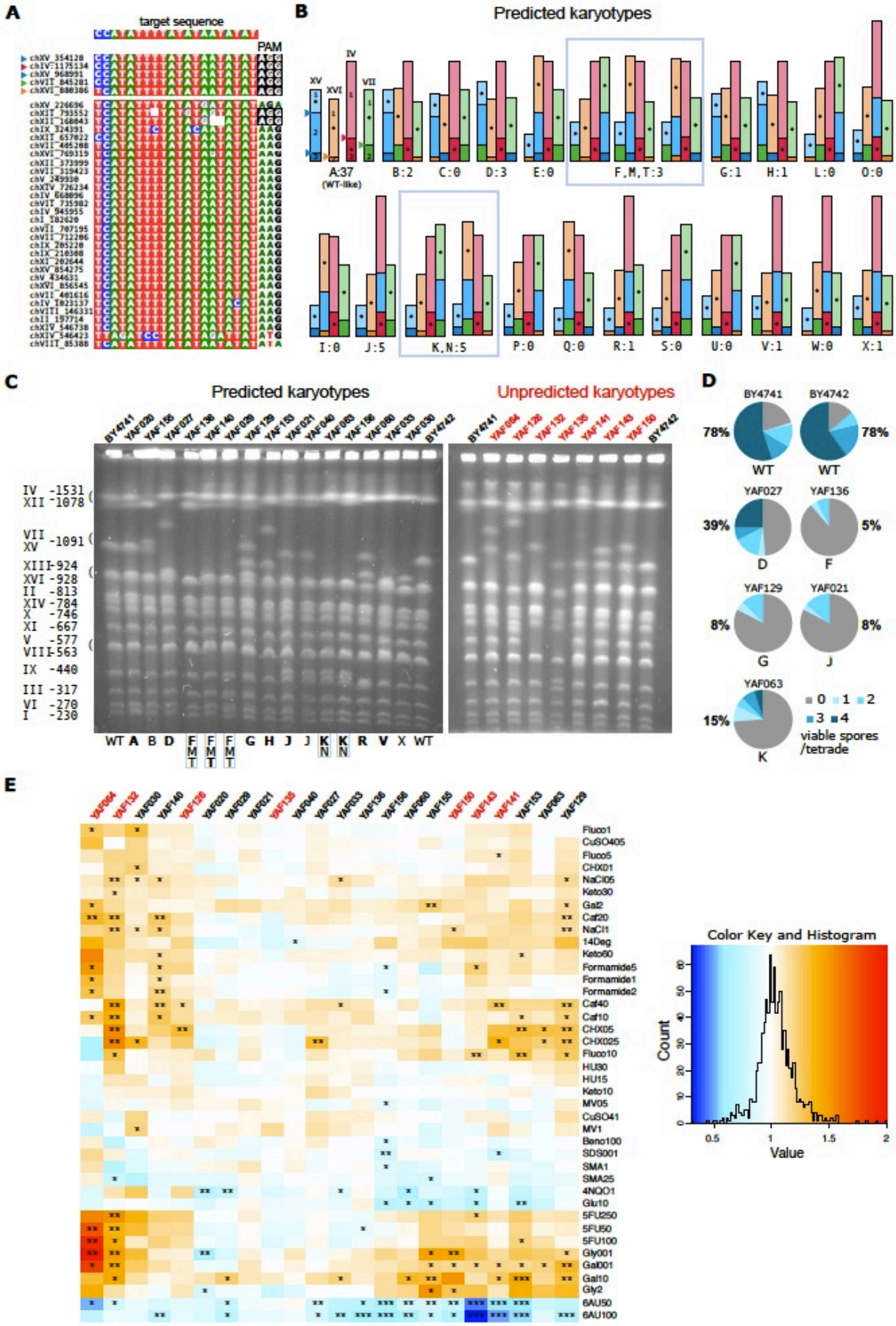

Figure 5: Induction of multiple rearrangements and phenotypic diversity of reshuffled strains. A. Multiple alignment of the target regions inTy3-LTR sequences. The gRNA target sequence is indicated on the top and the

375 corresponding homologous regions in the LTR are highlighted below. Associated PAM sequences are highlighted in
376 black. The five LTR sequences at the top are the best matches to the gRNA target sequence. Coordinates on the left
377 indicate the start of the corresponding TY3 LTRs. **B.** Predicted rearranged karyotypes (types A to X). Chromosomes are
378 represented proportionally to their size in kb. Centromeres are represented by black dots located in the middle of their
379 carrying fragment for readability. The chromosomal location of the 5 cutting sites corresponding to the 5 best matches to
380 the gRNA are indicated by colored triangles on the type A profile. The number of strains of each type that were
381 characterized by PFGE is indicated below each drawing. Types B to F have only 2 chimerical junctions resulting from a
382 single reciprocal translocation between 2 chromosomes. Types G to M have 3 chimerical junctions resulting from
383 translocations between 3 chromosomes (G, H, L, M) or the transposition of the chromosomal fragment XV.2 (I, J, K).
384 Types N to V have 4 chimerical junctions resulting from a combination of translocations and transpositions. Types W and
385 X have all 5 chimerical junctions. **C.** PFGE of 23 strains with predicted (left) and unpredicted (right) karyotypes. The
386 control WT strains (BY4741 and BY4742) are located on the most external lanes of each gel and their chromosome size
387 is indicated on the left. Strain names and types are indicated above and below the gels, respectively. The predicted types
388 are in bold when all chimerical junctions were validated by PCR. **D.** Percentage of viable spores and proportion of tetrads
389 with 0, 1, 2, 3, 4 viable spores obtained from crosses between BY (WT and rearranged) and WT SK1 strains. **E.**
390 Phenotypic variation among reshuffled strains. The heatmap represents the growth ratio of each strain (*i.e.* the colony
391 size on the tested conditions divided by its size on SC) divided by the growth ration of BY4741 or BY4742, depending on
392 the origin of the shuffled strain (Methods). The stars indicate the significant phenotypic effects (*, ** and *** indicate
393 pval<10^{-2}, 10^{-3} and 10^{-4}, respectively). Refer to supplementary fig 4 for the list of abbreviations corresponding to the 40
394 growth conditions. The strain names in red correspond to the unpredicted karyotypes in panel C.

395 Finally, we also recovered 37 type A strains that had a WT karyotype (fig 5B and C). For all of
396 them we validated the presence of all un-rearranged junctions by PCR. We sequenced the
397 junctions in 4 independent strains. We found that these strains underwent two different paths within
398 the same experiment. Firstly, 3 clones had all junctions identical to the original LTR sequences
399 with intact PAM, suggesting that Cas9 did not cut the target sites. Secondly, in the fourth clone, the
400 PAM sequences of three sequenced junctions were mutated, showing that the corresponding
401 chromosomes were cut and repaired yet without any rearrangement (supp fig 4). In this clone, one
402 junction could not be amplified, possibly because of a small-sized indel that could not be observed
403 on the PFGE profile.

404 **Exploring the phenotypic diversity of reshuffled strains**

405 It is well known that strains bearing heterozygous translocations have impaired meiosis resulting in
406 low spore viability [8,41–43]. We checked that crosses between rearranged and parental strains
407 indeed produced few viable spores (fig 5D). We tested 5 different strains with predicted rearranged

408 karyotypes and PCR-validated junctions. These strains were chosen because they encompassed
409 various rearrangements including reciprocal translocations between 2 and 3 chromosomes (types
410 D, F and G, respectively) and transpositions (types J and K). For each cross, we dissected 10
411 tetrads from two independent diploid strains (20 tetrads in total). The control strain without any
412 rearrangement shows 78% of viable spores with most tetrads harbouring 3 to 4 viable spores (fig
413 5D). By contrast, all heterozygous diploids had a severely impaired spore viability ranging from 5 to
414 39% with predominantly only 1 to 2 viable spores per tetrad. We observed no clear correlation
415 between the type of rearrangement and the impact on fertility. One strain carrying a single
416 reciprocal translocation between 2 chromosomes (type F) showed the lowest viability, comparable
417 to that of a more rearranged strain with 2 translocations between 3 chromosomes (type G). These
418 results show that knowing the type of rearrangements is not sufficient to predict their quantitative
419 impact on meiotic fertility, although most of them have a drastic negative effect.

420 Secondly, 22 rearranged strains (the 15 predicted and 7 unpredicted karyotypes presented on fig
421 5C) were phenotyped in 40 different growth conditions impacting various physiological processes
422 and in complete synthetic media as the reference condition. These 40 conditions include various
423 types of stresses, different drugs interfering with replication, transcription and translation as well as
424 compounds impacting several subcellular structures (supp table 4). In total, we performed 943
425 phenotypic measurements (fig 5E). We identified about twice as many cases where reshuffled
426 strains grew significantly faster compared to cases where they grew slower than the WT strain (91
427 and 48 cases, respectively), suggesting that genome shuffling might be advantageous in many
428 stressful conditions. The strongest phenotypic advantages of all corresponded to the strain with the
429 unpredicted karyotype harboring the 110 kb triplication (YAF064, see above) when DNA synthesis
430 is impaired (in the presence of the pyrimidine analog 5-fluorouracile) and in starvation (low carbon
431 concentration 0.01% of galactose or glycerol, fig 5E). However, none of 36 triplicated genes with a
432 known function is directly involved either in DNA synthesis or starvation, suggesting that the other
433 18 dubious ORFs present in this region could be involved in these phenotypes. More generally, for
434 the conditions that produce the greatest effects, most of the strains tended to react in a similar way.
435 For instance, in the presence of 6-azauracil (6AU), 4NQO and high glucose concentration all the
436 strains that showed a significant phenotypic variation grew slower than the WT while in the

437 presence of galactose, caffeine, cycloheximide and fluconazole all the strains that showed a
438 significant variation grew faster than the WT (fig 5E). Most strains (19 out of 22) showed variations
439 in at least 2 different conditions showing that genome shuffling is efficiently broadening the
440 phenotypic diversity. The most variable strain, YAF132, presented significant growth variations in
441 17 out of the 40 conditions (faster and slower than the WT in 15 and 2 conditions, respectively). By
442 opposition, the 2 type J strains (YAF021 and YAF040) as well as one strain with an unpredicted
443 karyotype (YAF135) showed no phenotypic variation in nearly all the 40 conditions. In conclusion,
444 these experiments revealed that reorganizing gene order along the chromosomes has direct
445 phenotypic consequences, including fitness advantage in many environmental conditions.

446

447 **DISCUSSION**

448 There are mounting evidences that SVs play a major role in phenotypic variation [44–46].
449 However, these genetic variants are the most difficult to interpret with respect to their functional
450 consequences. In this study, we developed a versatile CRISPR/Cas9-based method allowing to
451 engineer, with the same efficiency as point mutations, both uniquely targeted and multiple
452 reciprocal translocations. Our method therefore provides the possibility to quantify the role played
453 by structural variants in phenotypic diversity in a wide range of environmental conditions and in any
454 genetic background.

455 Targeted reciprocal translocations were obtained with a single-nucleotide precision by cloning pairs
456 of gRNAs that induce two concomitant DSBs in different chromosomes, which were repaired by
457 chimerical donor DNA (see fig 1A and B). After the translocation, the new chromosomal junctions
458 are not recognized by Cas9 which makes the mutation of the PAM sequence unnecessary. The
459 Cas9 plasmid is highly unstable and therefore can easily be cured from the strain which allows to
460 perform successive rounds of transformation to sequentially accumulate several targeted
461 translocations in the same genome. In addition, our methods also allow to introduce deletions at
462 the breakpoint concomitantly with the induction of the translocation.

463 The versatility of our approach allows to untangle the phenotypic impact of SVs from that of the
464 genetic background. We illustrated this with the translocation between the *SSU1* and *ECM34*
465 genes providing increased sulphite resistance to wine isolates, supposedly as a consequence of
466 sulphite supplementation in wine-making [40]. Engineering the same translocation in the BY4741
467 background resulted in decreased sulphite resistance. Therefore, the same translocation produces
468 two opposite phenotypes in the laboratory and the wine backgrounds. It was previously reported
469 that the two strains also differ by a 76 bp repeated motif in the promoter of *ECM34* and that
470 sulphite resistance correlated with the number of repeats [40]. Adding the four copies of the wine
471 promoter into the translocated BY4741 strain that is devoid of repeats resulted in increased
472 sulphite resistance, confirming that the repeats rather than the translocation are responsible for
473 sulphite resistance. However, sulphite resistance remained lower in the laboratory as compared to
474 the wine isolate despite they share both the same translocation and promoter repeats. This
475 strongly suggests that additional polymorphisms such as SNPs also contribute to sulphite

476 resistance in the wine isolate. For instance, there are 4 non-synonymous SNPs in the coding
477 sequence of *SSU1* between the 2 genetic backgrounds. These findings provide a striking example
478 of the advantages brought by our technique to untangle the phenotypic impact of SVs from that of
479 the genetic background.

480 Multiple translocations were obtained by using a single gRNA that targets dispersed repeat
481 sequences leading to a large diversity of karyotypes. These results show that the genotypic space
482 accessible by such an approach is probably very large. Our genome reshuffling procedure is
483 reminiscent of the restructuring technology developed by Muramoto and collaborators [47] that
484 uses a temperature-dependent endonuclease to conditionally induce multiple DSBs in the genome
485 of yeast and *A. thaliana*. However, our method is potentially more versatile because we can target
486 different types of repeated sequences with variable locations (within or between genes,
487 subtelomeric or internal, etc) and variable copy numbers. By analyzing the genome of *S. cerevisiae*
488 for repeated gRNA target sequences, we identified 39,374 repeated targets with varying number of
489 occurrences in the genome (from 2 to 59). Repeated targets were mostly found within Ty
490 transposable elements (11,503) and protein coding genes (10,368 in 479 genes located in all 16
491 chromosomes). Interestingly, we also found 3,438 repeated target gRNA located in intergenic
492 regions which should allow to rearrange chromosomes without disrupting coding sequences. In
493 addition, our CRISPR/Cas9 shuffling procedure is doable in any genetic background and therefore
494 potentially more versatile than the Cre/Lox based SCRaMbLE techniques that can be used only in
495 yeast strains with synthetic chromosomes.

496 Given the location of the multiple DSBs induced by the Ty3 LTR gRNA we chose and considering
497 that all viable rearranged chromosomes must have a single centromere, we could predict the
498 formation of 23 rearranged karyotypes (types B to X in fig 5B). These translocations result from
499 trans repair between targeted DSBs (*i.e.* two DNA ends from two different DSBs are repaired
500 together) without any crossover within the uncut LTRs used as template (fig 1C). We isolated 23
501 strains representing 10 different predicted karyotypes (fig 5C). The observed distribution of all
502 predicted types, except type J, was very similar to the expected frequency of each types,
503 suggesting that DSBs were repaired in a random way and that no specific chromosomal contact
504 would be favored during repair. It is interesting to note that type J corresponds to the only

505 chromosomal combination amongst all discernible predicted types where chromosome XVI
506 remains non-rearranged (fig 5B). The target sequence on chromosome XVI is the only one that
507 contains a mismatch with the gRNA sequence (fig 5A), suggesting that even a single mismatch
508 located on the 5' end of the target sequence could be sufficient to decrease the cutting efficiency
509 contrarily to *in vitro* results showing that mismatches at the last two nucleotides at the PAM distal
510 region show similar or even higher cleavage efficiency than that of WT target [48,49]. We also
511 isolated 7 strains with rearranged karyotypes different from the 23 predicted profiles (fig 5C). Such
512 rearrangements are believed to result from crossovers involving uncut LTRs (fig 1C), leading to
513 translocations involving uncut chromosomes. The large number of LTRs that can be used for each
514 repair event explains why these karyotypes would be difficult to predict. Moreover, we cannot
515 exclude that some of the unpredicted karyotypes would also result from untargeted LTRs being cut
516 by CRISPR/Cas9. However, this scenario seems very unlikely because all other LTRs are devoid
517 of PAM and/or contain multiple mutations and indels in the target sequence (fig 5A). Another
518 possible explanation to the presence of unpredicted karyotypes would be multipartite ectopic
519 recombination between cut and uncut chromosomes where a single end of a DSB can invade
520 multiple sequences located on intact chromosomes during its search for homology leading to
521 translocations between uncut chromosomes by multi-invasion-induced rearrangement [50].
522 Surprisingly, more complex rearrangements involving large duplications were also recovered (fig
523 5C, supp fig 5), showing that inducing DSB can trigger the formation of large duplicated segments,
524 as previously described [51]. Consistently, it has been shown that BIR can occur by several rounds
525 of strand invasion, DNA synthesis and dissociation within dispersed repeated sequences such as
526 LTRs, leading to chromosome rearrangements [52]. One such example was found here in the
527 strain with the large segmental triplication where one chimerical junction probably resulted from
528 template switching between the Ty3 LTR and the full-length Ty2 elements found in the vicinity of
529 the CRISPR-induced DSBs (supp fig 5).
530 We determined the phenotypes of strains carrying multiple rearrangements both in mitotic and
531 meiotic conditions. We showed that crosses between rearranged and parental strains produced
532 very few viable spores (fig 5D), supporting earlier studies revealing that meiotic pairing and
533 segregation is impaired in diploid strains bearing heterozygous translocations [8,41–43]. We also

534 showed that genome reshuffling generates a great phenotypic diversity under specific
535 environmental conditions including many cases of fitness advantage (fig 5E). Similar findings were
536 previously described both in *S. cerevisiae* [53,54] and *Schizosaccharomyces pombe* [8,46].
537 However, for the first time in this study all rearrangements are completely markerless and scarless
538 (no CRE/Lox site) and for the predicted karyotypes no gene was disrupted nor duplicated
539 suggesting that balanced rearrangements between repeated sequences such as Ty3 LTRs, simply
540 reconfiguring the chromosome architecture are sufficient to create fitness diversity. Ty3 LTRs
541 control expression of the Ty3 genomic RNA and have an organization similar to other yeast
542 promoters. Ty3 LTRs contain positive control elements for pheromone induction, negative control
543 elements for mating-type and also pheromone-independent transcriptional activity [55]. The
544 transcriptional activity of Ty3 LTRs could possibly explain the observed phenotypic diversity
545 associated with genome reshuffling at these sites. Interestingly, the presence of the nucleotide-
546 depleting drug 6AU induces the strongest growth defect of all tested conditions (fig 5E). Sensitivity
547 to 6AU is a well-documented phenotype associated with transcription-elongation mutants, reducing
548 both the elongation rate and processivity [56–59], suggesting that transcription might be globally
549 affected in the reshuffled strains. Further work is needed to decipher the molecular mechanisms at
550 the origin of the phenotypic diversity associated with genome reshuffling.
551

552 **METHODS**

553 **Strains and media**

554 The strains of *Saccharomyces cerevisiae* BY4741, (*MAT*a, *his3Δ1*, *leu2Δ0*, *ura3Δ0*, *met15Δ0*) and
555 BY4742 (*MAT*α, *his3Δ1*, *leu2Δ0*, *ura3Δ0*, *lys2Δ0*) were used for generating both targeted and
556 multiple translocations. Pre-cultures were performed in YPD (yeast extract 10 $g.l^{-1}$ peptone 20 $g.l^{-1}$,
557 glucose 20 $g.l^{-1}$) or in SC (Yeast Nitrogen Base with ammonium sulfate 6.7 $g.l^{-1}$, amino acid
558 mixture 2 $g.l^{-1}$, glucose 20 $g.l^{-1}$) for high-throughput phenotyping experiments. After transformation,
559 cells were selected on SC medium depleted in leucine. The SK1 strains SKY1513 (*MAT*α*,*
560 *ho::LYS2*, *ura3*, *leu2::HISG*, *lys2*, *arg4*(Nnde1)-Nsp, *thr1-A*, *SPO11*-HA3-His6::*KanMX4*) and
561 SKY1708 (*MAT*a, *ho::LYS*2, *ura3*, *leu2::HISG, lys2*, *arg4*-Bgl::NdeI-site1°, *CEN8::URA3*) were
562 used for their high sporulation efficiency compared to BY strains [60] to perform crosses and to
563 quantify spore viability of the rearranged strains. Sulphite resistance of our engineered strains
564 (YAF202 and YAF158) was compared in liquid assay to that of wine strains DBVPG6765 (provided
565 by Gianni Liti (IRCAN, Nice)) and Y9J_1b and to the BY4741 strain. Cells were grown overnight in
566 YPD broth prior to inoculation at a concentration of 10^4 cells/mL in 8ml of YPD broth buffered at
567 pH=4 with tartaric acid and containing Na_2SO_3 concentrations ranging from 0 to 20 mM [61]. The
568 50 ml culture tubes were tightly closed to avoid evaporation of sulphites and incubated at 30°C.
569 Photographs and OD_{600} were taken after 48 hours to quantify cell growth. Plasmid cloning steps
570 were performed in chemically competent *Escherichia coli* DH5α. Ampicillin resistant bacteria were
571 selected on LB medium supplemented with ampicillin at 100 µg/ml.

572 **Identification of CRISPR/Cas9 target sequences**

573 For the translocation between *ADE2* and *CAN1*, the target sequences CAN.Y and ADE2.Y found in
574 the literature [27] were re-used. The new targets formed by the first translocation were targeted to
575 "reverse" the translocation and restore the original junctions. For the *ECM34*/*SSU1* translocation,
576 specific CRISPR/Cas9 target sequences with minimal off-targets were chosen as close as possible
577 to the natural recombination site of wine strains with the CRISPOR v4.3 website
578 (http://crispor.tefor.net) using the reference genome of *Saccharomyces cerevisiae* (UCSC Apr.
579 2011 SacCer_Apr2011/sacCer3) and the NGG protospacer adjacent motif. For multiple
580 rearrangements, we identified 39 occurrences of Ty3-LTRs in the latest version of the genome of

581 *Saccharomyces cerevisiae* S288C (accession number GCF_000146045.2), which we have aligned
582 using MUSCLE. Four sequences were incomplete and excluded from further analysis. We then
583 manually selected a suitable gRNA sequence targeting five Ty3-LTR elements and looked for off-
584 targets to this target sequence with CRISPOR. Predicted off-targets had either mismatches with
585 the chosen guide and/or were devoid of PAM indicating that they would not be recognized by
586 CRISPR/Cas9.

587 **Construction of CRISPR/Cas9 plasmids with one or two guides**

588 The original plasmid pGZ110 was kindly provided by Bruce Futcher (Gang Zhao, Justin Gardin,
589 Yuping Chen, and Bruce Futcher, Stony Brook University; personal communication). All plasmids
590 constructed in this study were obtained by cloning in pGZ110 either a 430 bp DNA fragment
591 reconstituting a two-gRNA expression cassette or a 20 bp fragment corresponding to the target
592 sequence of a single gRNA (fig 1a). We linearised pGZ110 with the enzyme LguI (ThermoFischer
593 FD1934) and gel purified the backbone. In order to clone a single 20 bp target sequence we first
594 annealed two oligonucleotides of 23 bases with 5' overhangs of 3 bases complementary to the
595 LguI sites. Annealing was performed by mixing equimolar amounts of forward and reverse
596 oligonucleotides at 100 pmol/µl with NEBuffer 4 (New England Biolabs), heating 5 minutes at 95°C
597 and allowing the mix to cool down slowly to room temperature. We then mixed 100 ng of backbone
598 with 20 pmol of double stranded insert and performed the ligation with the Thermo Fischer Rapid
599 DNA ligation Kit (K1422) according to manufacturer instructions. In order to obtain plasmids with
600 an expression cassette containing two gRNAs, we ordered a 464 bp synthetic DNA fragment
601 composed of a 430 bp sequence containing the target sequence of the first gRNA, its structural
602 component and its terminator sequence followed by the promoter of the second gRNA and its
603 target sequence, flanked by two LguI sites in opposite orientation (fig 1a). This 464 bp DNA
604 fragment was digested with LguI to obtain the 430 bp insert with adequate 5' overhangs of 3 bases
605 and gel-purified for ligation in pGZ110. We mixed 100 ng of backbone and 20 ng of insert and
606 performed ligation as explained previously. As an alternative to the ordering a synthetic DNA
607 fragment, the double gRNA cassette can easily be PCR amplified using as template any plasmid
608 already containing two gRNAs and two 55 bp oligonucleotides. The first oligo is composed of the
609 LguI site (15 bp), the gRNA target sequence 1 (20 bp) and a homology region to the structural

610 component of the gRNA 1 (20 bp). The second oligo is composed of the LguI site (15 bp), the
611 gRNA target sequence 2 (20 bp) and a homology region to the promoter region of the gRNA 2
612 (20 bp). The resulting PCR product is then digested by LguI and cloned in the vector as previously
613 described.
614 All oligonucleotides and synthetic DNA fragments were ordered from Eurofins. Refer to
615 supplementary material for oligonucleotides and synthetic DNA sequences (supp table 1).

616 **Yeast transformation**

617 Yeast cells were transformed using the standard lithium acetate method [62] with modifications.
618 Per transformation, 10^8 cells in Log phase were washed twice in 1 mL of double distilled water,
619 then washed twice in 1 mL of lithium acetate mix (lithium acetate 0.1 M, TE) and cells were
620 recovered in 50 μL of lithium acetate mix. To this mix 50 μg of denatured salmon sperm
621 (Invitrogen), 500 ng of Cas9 plasmid, and 5 μL of double-stranded DNA donors for repair of
622 CRISPR-induced DSBs were added. Double-stranded DNA donors for repair were prepared by
623 mixing equimolar amounts of forward and reverse oligonucleotides at 100 pmol/µl with NEBuffer 4
624 (New England Biolabs), heating 5 minutes at 95°C and allowing the mix to cool down slowly to
625 room temperature. Transformation were performed by adding 300 μL of lithium acetate/PEG
626 solution (lithium acetate 0.1 M, PEG4000 45 %, TE), then by vortexing for 1 minute and finally
627 incubating the cells for 25 minutes at 42°C. After transformation, cells were plated on YPD to
628 check for viability and on synthetic medium depleted of leucine to select for transformants. Plates
629 were incubated 4 days at 30°C. To determine the canavanine phenotypes of the transformants,
630 137 and 114 pink colonies from the RT and PM experiments, respectively, were resuspended in
631 water and spot tests realized on SC and SC-arg plus canavanine (60 mg/L) agar plates. Plates
632 were incubated 4 days at 30C before scoring the CanR/CanS phenotypes Similar tests were
633 performed for the 7 and 30 white transformants obtained from the RT and PM experiments,
634 respectively (fig 2B).

635 **Plasmid Stability**

636 The pGZ110 plasmid is highly unstable when selection for the *LEU2* gene is removed. To cure the
637 plasmid cell were grown overnight in YPD at 30°C. Ten individual cells were micromanipulated on
638 YPD plates with the MSM400 micromanipulator (Singer Instruments) and grown at 30°C for 2

639 days. Colonies were then serially replicated on CSM-Leu and YPD. All 10 colonies lost the ability
640 to grow on CSM-Leu.

641 **Estimation of CRISPR/Cas9 transformation, cutting and repair efficiencies**

642 Efficiencies were calculated on 3 replicates of the *ADE2*/*CAN1* experiments. Transformation
643 efficiency was defined as p/T with p being the average number of transformants obtained with
644 Cas9 plasmid bearing no gRNA and without donor DNA and T being the average number of
645 transformed cells. Cutting efficiency (%) was defined as $100*(p-g)/p$ with g being the average
646 number of transformants obtained with Cas9 plasmid with the gRNAs and without donor DNA.
647 Repair efficiency (%) was defined as $100*d/(p-g)$ with d being the average number of transformants
648 obtained with Cas9 plasmid with the gRNAs and with donor DNAs (fig 2B).

649 **PFGE and colony PCR for karyotyping rearranged strains**

650 Whole yeast chromosomes agarose plugs were prepared according to a standard method [63] and
651 sealed in a 1% Seakem GTC agarose and 0.5x TBE gel. PFGE was conducted with the CHEF-
652 DRII (BioRad) system with the following program: 6 V/cm for 10 hours with a switching time of 60
653 seconds followed by 6 V/cm for 17h with switching time of 90 seconds. The included angle was
654 120° for the whole duration of the run. We compared observed karyotypes with expected
655 chromosome sizes and tested the chromosomal junctions by colony PCR with ThermoFischer
656 DreamTaq DNA polymerase.

657 **Southern blot validation of *ECM34*/*SSU1* translocation**

658 Southern blot was used to validate the translocation between *ECM34* (ch. VIII) and *SSU1* (ch. XVI).
659 Genomic DNA was extracted from BY4741 and the engineered strain YAF082 using the Qiagen
660 DNA buffer set (19060) and Genomic-tip 100/G (10243) according to manufacturer instructions and
661 further purified and concentrated by isopropanol precipitation. Digestion of 10 µg of genomic DNA
662 per strain/probe assay was carried out using FastDigest EcoRI (ThermoFischer FD0274).
663 Electrophoresis, denaturation and neutralisation of the gel were performed according to
664 established procedure [64]. Transfer on nylon membrane (Amersham Hybond XL) was performed
665 using the capillarity setup [65]. The membrane was UV-crosslinked with the Stratalinker 1800
666 device in automatic mode. Probes targeting the genes YHL044W and *ARN1* located upstream and

667 downstream of the cutting site in the *ECM34* promoter respectively and the genes *NOG1* and
668 *SSU1* located upstream and downstream of the cutting site in the *SSU1* promoter respectively
669 were amplified with ThermoFischer DreamTaq, DIG-11-dUTP deoxyribonucleotides (Roche 11 175
670 033 910) and gel purified. Blotting and revelation were conducted using the Roche DIG High Prime
671 DNA Labelling and Detection Starter kit II (11 585 614 910) according to manufacturer instructions.
672 Imaging was performed using the G:BOX Chemi XT4 (Syngene) with CSPD chemiluminescence
673 mode. All oligonucleotides are described in supp table 1.

674 **Oxford Nanopore *de-novo* genome assembly**

675 DNA from strains YAF019 and YAF064 was extracted using QIAGEN Genomic-tip 20/G columns
676 and sheared using covaris g-TUBEs for average reads lengths of 8 kb and 15 kb respectively. DNA
677 was repaired and dA-tailed using PreCR and FFPE kits (New England Biolabs) and cleaned with
678 Ampure XP beads (Beckman Coulter). SQK-LSK108 adapters were ligated and libraries run on
679 FLO-MIN107 R9.5 flowcells. Raw signals were basecalled locally using Albacore v2.0.2 with
680 default quality filtering. Flowcell outputs are shown in supp table 2.
681 YAF019 was assembled using the LRSDAY v1 pipeline [66], including nanopolish v0.8.5 correction
682 and excluding pilon polishing due to lack of illumina data. Due to only 19x coverage, the
683 correctedErrorRate for Canu assembly was increased to 0.16. Assembly data are shown in supp
684 table 3. YAF064 was processed using the LRSDAY v1 pipeline [66]. Linear chromosomes were
685 assembled by SMARTdenovo v1 using 40x coverage of the longest Canu-corrected reads and
686 combined with a Canu assembled mitochondrial genome. For canu correction, due to 200x
687 coverage, correctedErrorRate was set at 0.75. All corrected reads were aligned against a
688 reference-quality S288C genome, assembled with PacBio reads [67] using LAST-921. Split reads
689 were used to highlight structural variations not apparent in the SMARTdenovo assembly. Read
690 coverage was used to calculate an increase in the number of copies of particular regions within the
691 rearranged genome. Evidence of rearrangements defined by overlapping reads and changes in
692 copy number were used to manually adjust the assembly prior to nanopolish v0.8.5 and Pilon
693 v1.22 error correction.

694

695 **Spore viability**

696 Colonies of rearranged strains originating from the BY background and SK1 strains of the opposed
697 mating type were mixed and spread on the same YPD plate and left overnight at 30°C. The next
698 day, the cells were re-suspended in distilled water and single cells were picked using the Sanger
699 MSM 400 micro-manipulator and left to grow on YPD for 2 days at 30°C until a colony appeared.
700 Colonies originating from single cells were replicated on sporulation medium and left for 4 to 7
701 days at 30°C until tetrad appeared. For each cross, 10 tetrads from two diploid strains were
702 dissected on YPD and left to grow for 3 days before counting viable spores.

703 **High-throughput phenotyping**

704 Quantitative phenotyping was performed using endpoint colony growth on solid media. First,
705 strains were grown overnight on liquid YPD medium then pinned onto a solid SC medium with a
706 1,536 colony per plate density format using robot assisted pinning with ROTOR™ (Singer
707 Instrument) and incubated overnight at 30°C. Once sufficient growth is achieved, the matrix plate is
708 replicated onto 40 media conditions (supp table 4) plus SC as a pinning control. Plates were
709 incubated at 30°C (except for the 14°C phenotyping). After 24h, plates were imaged at a 12Mpixel
710 resolution. Quantification of the colony size was performed in R using Gitter [68]. Raw sizes were
711 corrected using two successive corrections: a spatial smoothing was applied to the colony size
712 [69]. This allowed to account for variation of the plate thickness. Another correction was then
713 applied to rescale colony size by row and column [69] which is important for colonies lying at the
714 edges of the plate thus having easier access to nutrients compared to strains in the center. All
715 calculations were performed using R. Once the corrected sizes were obtained, the growth ratio of
716 each colony was computed as the colony size on the tested conditions divided by its size on SC.
717 To detect the phenotypic effect of the engineered translocations, each growth ratio has been
718 normalized by the growth ratio of BY4741 or BY4742, depending on the origin of the shuffled
719 strain, on the 40 tested condition. As each strain was present six time, the value considered for its
720 phenotype was the median of all its replicates thus smoothing pinning heterogeneity. Each
721 experiment was repeated 2 times independently in the 40 growth conditions. Correlations between
722 the two replicate experiments are presented in supp fig 6. For each replicate experiment and
723 condition, the growth ratios of the 6 colonies of each tested strain were compared to the growth

724 ratio of the reference colonies (BY4741 or BY4742) and a Wilcoxon test was used determined the
725 significance of the phenotypic effect: ***, ** and * indicated that the two p-values from both
726 replicates were lower than 10^{-4}, 10^{-3} and 10^{-2}, respectively.

727 **DATA ACCESS**

728 The Oxford Nanopore sequencing data are deposited in the Sequence Read Archive under the
729 project number (accession number pending).

730 **ACKNOWLEDGMENTS**

731 We are grateful to Bruce Futcher and Gang Zhao (Stony Brook University, USA) for providing the
732 pGZ110 plasmid. We thank our colleagues, Gianni Liti (IRCAN, France) and Bertrand Llorente
733 (CRCM, France) for fruitful discussions and constructive suggestions as well as for providing us
734 the wine and SK1 strains. We are also grateful to Maëlys Born-Bony for her experimental help.
735 This work was supported by the Agence Nationale de la Recherche [ANR-16-CE12-0019]. T.F. is
736 supported by a fellowship from the medical association la Fondation pour la Recherche Médicale.
737 J.S. is a member of the Institut Universitaire de France.

738

739

740 **REFERENCES**

741 1. Argueso JL, Westmoreland J, Mieczkowski PA, Gawel M, Petes TD, Resnick MA. Double-
742 strand breaks associated with repetitive DNA can reshape the genome. Proc Natl Acad Sci U S A.
743 2008;105: 11845–11850. doi:10.1073/pnas.0804529105
744 2. Piazza A, Wright WD, Heyer W-D. Multi-invasions Are Recombination Byproducts that
745 Induce Chromosomal Rearrangements. Cell. 2017;170: 760–773.
746 3. Branzei D, Foiani M. Regulation of DNA repair throughout the cell cycle. Nat Rev Mol Cell
747 Biol. 2008;9: 297–308. doi:10.1038/nrm2351
748 4. Fairhead C, Llorente B, Denis F, Soler M, Dujon B. New vectors for combinatorial deletions
749 in yeast chromosomes and for gap-repair cloning using “split-marker” recombination. Yeast
750 Chichester Engl. 1996;12: 1439–1457. doi:10.1002/(SICI)1097-0061(199611)12:14<1439::AID-
751 YEA37>3.0.CO;2-O
752 5. Richardson C, Jasin M. Frequent chromosomal translocations induced by DNA double-
753 strand breaks. Nature. 2000;405: 697–700. doi:10.1038/35015097
754 6. Storici F, Resnick MA. The delitto perfetto approach to in vivo site-directed mutagenesis
755 and chromosome rearrangements with synthetic oligonucleotides in yeast. Methods Enzymol.
756 2006;409: 329–345. doi:10.1016/S0076-6879(05)09019-1
757 7. Delneri D, Colson I, Grammenoudi S, Roberts IN, Louis EJ, Oliver SG. Engineering
758 evolution to study speciation in yeasts. Nature. 2003;422: 68–72. doi:10.1038/nature01418
759 8. Avelar AT, Perfeito L, Gordo I, Ferreira MG. Genome architecture is a selectable trait that
760 can be maintained by antagonistic pleiotropy. Nat Commun. 2013;4: 2235.
761 doi:10.1038/ncomms3235
762 9. Naseeb S, Carter Z, Minnis D, Donaldson I, Zeef L, Delneri D. Widespread Impact of
763 Chromosomal Inversions on Gene Expression Uncovers Robustness via Phenotypic Buffering. Mol
764 Biol Evol. 2016;33: 1679–1696.
765 10. Naseeb S, Delneri D. Impact of Chromosomal Inversions on the Yeast DAL Cluster. J Mata
766 PLoS ONE. 2012;7: 42022.
767 11. Annaluru N, Muller H, Mitchell LA, Ramalingam S, Stracquadanio G, Richardson SM, et al.
768 Total Synthesis of a Functional Designer Eukaryotic Chromosome. Science. 2014;344: 55–58.
769 doi:10.1126/science.1249252
770 12. Hochrein L, Mitchell LA, Schulz K, Messerschmidt K, Mueller-Roeber B. L-SCRaMbLE as a
771 tool for light-controlled Cre-mediated recombination in yeast. Nat Commun. 2018;9.
772 doi:10.1038/s41467-017-02208-6
773 13. Jia B, Wu Y, Li B-Z, Mitchell LA, Liu H, Pan S, et al. Precise control of SCRaMbLE in
774 synthetic haploid and diploid yeast. Nat Commun. 2018;9: 1933. doi:10.1038/s41467-018-03084-4
775 14. Shen Y, Stracquadanio G, Wang Y, Yang K, Mitchell LA, Xue Y, et al. SCRaMbLE
776 generates designed combinatorial stochastic diversity in synthetic chromosomes. Genome Res.
777 2016;26: 36–49. doi:10.1101/gr.193433.115
778 15. Blount BA, Gowers G-OF, Ho JCH, Ledesma-Amaro R, Jovicevic D, McKiernan RM, et al.
779 Rapid host strain improvement by in vivo rearrangement of a synthetic yeast chromosome. Nat
780 Commun. 2018;9. doi:10.1038/s41467-018-03143-w
781 16. Luo Z, Wang L, Wang Y, Zhang W, Guo Y, Shen Y, et al. Identifying and characterizing
782 SCRaMbLEd synthetic yeast using ReSCuES. Nat Commun. 2018;9. doi:10.1038/s41467-017-
783 00806-y
784 17. Shen MJ, Wu Y, Yang K, Li Y, Xu H, Zhang H, et al. Heterozygous diploid and interspecies
785 SCRaMbLEing. Nat Commun. 2018;9: 1934. doi:10.1038/s41467-018-04157-0
786 18. Muramoto N, Oda A, Tanaka H, Nakamura T, Kugou K, Suda K, et al. Phenotypic
787 diversification by enhanced genome restructuring after induction of multiple DNA double-strand
788 breaks. Nat Commun. 2018;9: 1995. doi:10.1038/s41467-018-04256-y
789 19. Brunet E, Simsek D, Tomishima M, DeKelver R, Choi VM, Gregory P, et al. Chromosomal
790 translocations induced at specified loci in human stem cells. Proc Natl Acad Sci. 2009;106: 10620–
791 10625. doi:10.1073/pnas.0902076106
792 20. Piganeau M, Ghezraoui H, De Cian A, Guittat L, Tomishima M, Perrouault L, et al. Cancer
793 translocations in human cells induced by zinc finger and TALE nucleases. Genome Res. 2013;23:
794 1182–1193. doi:10.1101/gr.147314.112
795 21. Richard G-F, Viterbo D, Khanna V, Mosbach V, Castelain L, Dujon B. Highly Specific

Contractions of a Single CAG/CTG Trinucleotide Repeat by TALEN in Yeast. Ashizawa T, editor. PLoS ONE. 2014;9: e95611. doi:10.1371/journal.pone.0095611
22. Xiao A, Wang Z, Hu Y, Wu Y, Luo Z, Yang Z, et al. Chromosomal deletions and inversions mediated by TALENs and CRISPR/Cas in zebrafish. Nucleic Acids Res. 2013;41: e141–e141. doi:10.1093/nar/gkt464
23. Doudna JA, Charpentier E. The new frontier of genome engineering with CRISPR-Cas9. Science. 2014;346: 1258096–1258096. doi:10.1126/science.1258096
24. Fraczek MG, Naseeb S, Delneri D. History of genome editing in yeast. Yeast. 2018;35: 361–368. doi:10.1002/yea.3308
25. Alexander WG. A history of genome editing in Saccharomyces cerevisiae. Yeast Chichester Engl. 2018;35: 355–360. doi:10.1002/yea.3300
26. Wang F, Qi LS. Applications of CRISPR Genome Engineering in Cell Biology. Trends Cell Biol. 2016;26: 875–888. doi:10.1016/j.tcb.2016.08.004
27. DiCarlo JE, Norville JE, Mali P, Rios X, Aach J, Church GM. Genome engineering in Saccharomyces cerevisiae using CRISPR-Cas systems. Nucleic Acids Res. 2013;41: 4336–4343. doi:10.1093/nar/gkt135
28. Jakočiūnas T, Bonde I, Herrgård M, Harrison SJ, Kristensen M, Pedersen LE, et al. Multiplex metabolic pathway engineering using CRISPR/Cas9 in Saccharomyces cerevisiae. Metab Eng. 2015;28: 213–222. doi:10.1016/j.ymben.2015.01.008
29. Mans R, van Rossum HM, Wijsman M, Backx A, Kuijpers NGA, van den Broek M, et al. CRISPR/Cas9: a molecular Swiss army knife for simultaneous introduction of multiple genetic modifications in Saccharomyces cerevisiae. FEMS Yeast Res. 2015;15. doi:10.1093/femsyr/fov004
30. Mans R, Wijsman M, Daran-Lapujade P, Daran J-M. A protocol for introduction of multiple genetic modifications in Saccharomyces cerevisiae using CRISPR/Cas9. FEMS Yeast Res. 2018; doi:10.1093/femsyr/foy063
31. Sasano Y, Nagasawa K, Kaboli S, Sugiyama M, Harashima S. CRISPR-PCS: a powerful new approach to inducing multiple chromosome splitting in Saccharomyces cerevisiae. Sci Rep. 2016;6. doi:10.1038/srep30278
32. Luo J, Sun X, Cormack BP, Boeke JD. Karyotype engineering by chromosome fusion leads to reproductive isolation in yeast. Nature. 2018;560: 392–396. doi:10.1038/s41586-018-0374-x
33. Shao Y, Lu N, Wu Z, Cai C, Wang S, Zhang L-L, et al. Creating a functional single-chromosome yeast. Nature. 2018;560: 331–335. doi:10.1038/s41586-018-0382-x
34. Bao Z, Xiao H, Liang J, Zhang L, Xiong X, Sun N, et al. Homology-Integrated CRISPR–Cas (HI-CRISPR) System for One-Step Multigene Disruption in *Saccharomyces cerevisiae*. ACS Synth Biol. 2015;4: 585–594. doi:10.1021/sb500255k
35. Roy KR, Smith JD, Vonesch SC, Lin G, Tu CS, Lederer AR, et al. Multiplexed precision genome editing with trackable genomic barcodes in yeast. Nat Biotechnol. 2018; doi:10.1038/nbt.4137
36. Sadhu MJ, Bloom JS, Day L, Siegel JJ, Kosuri S, Kruglyak L. Highly parallel genome variant engineering with CRISPR/Cas9 in eukaryotic cells. 2017; doi:10.1101/147637
37. Després PC, Dubé AK, Nielly-Thibault L, Yachie N, Landry CR. Double Selection Enhances the Efficiency of Target-AID and Cas9-Based Genome Editing in Yeast. G3 Genes Genomes Genet. 2018;8: 3163–3171. doi:10.1534/g3.118.200461
38. Maddalo D, Manchado E, Concepcion CP, Bonetti C, Vidigal JA, Han Y-C, et al. In vivo engineering of oncogenic chromosomal rearrangements with the CRISPR/Cas9 system. Nature. 2014;516: 423–427. doi:10.1038/nature13902
39. Vanoli F, Tomishima M, Feng W, Lamribet K, Babin L, Brunet E, et al. CRISPR-Cas9–guided oncogenic chromosomal translocations with conditional fusion protein expression in human mesenchymal cells. Proc Natl Acad Sci. 2017;114: 3696–3701. doi:10.1073/pnas.1700622114
40. Pérez-Ortín JE, Querol A, Puig S, Barrio E. Molecular characterization of a chromosomal rearrangement involved in the adaptive evolution of yeast strains. Genome Res. 2002;12: 1533–1539. doi:10.1101/gr.436602
41. Hou J, Friedrich A, de Montigny J, Schacherer J. Chromosomal rearrangements as a major mechanism in the onset of reproductive isolation in Saccharomyces cerevisiae. Curr Biol CB. 2014;24: 1153–1159. doi:10.1016/j.cub.2014.03.063
42. Loidl J, Jin QW, Jantsch M. Meiotic pairing and segregation of translocation quadrivalents in yeast. Chromosoma. 1998;107: 247–254.
43. Liti G, Barton DBH, Louis EJ. Sequence Diversity, Reproductive Isolation and Species

Concepts in Saccharomyces. Genetics. 2006;174: 839–850.
44. Gabur I, Chawla HS, Snowdon RJ, Parkin IAP. Connecting genome structural variation with complex traits in crop plants. TAG Theor Appl Genet Theor Angew Genet. 2019;132: 733–750. doi:10.1007/s00122-018-3233-0
45. Girirajan S, Eichler EE. Phenotypic variability and genetic susceptibility to genomic disorders. Hum Mol Genet. 2010;19: R176-187. doi:10.1093/hmg/ddq366
46. Jeffares DC, Jolly C, Hoti M, Speed D, Shaw L, Rallis C, et al. Transient structural variations have strong effects on quantitative traits and reproductive isolation in fission yeast. Nat Commun. 2017;8: 14061. doi:10.1038/ncomms14061
47. Muramoto N, Oda A, Tanaka H, Nakamura T, Kugou K, Suda K, et al. Phenotypic diversification by enhanced genome restructuring after induction of multiple DNA double-strand breaks. Nat Commun. 2018;9.
48. Fu BXH, Hansen LL, Artiles KL, Nonet ML, Fire AZ. Landscape of target:guide homology effects on Cas9-mediated cleavage. Nucleic Acids Res. 2014;42: 13778–13787. doi:10.1093/nar/gku1102
49. Zeng Y, Cui Y, Zhang Y, Zhang Y, Liang M, Chen H, et al. The initiation, propagation and dynamics of CRISPR-SpyCas9 R-loop complex. Nucleic Acids Res. 2018;46: 350–361. doi:10.1093/nar/gkx1117
50. Piazza A, Wright WD, Heyer W-D. Multi-invasions Are Recombination Byproducts that Induce Chromosomal Rearrangements. Cell. 2017;170: 760-773.e15. doi:10.1016/j.cell.2017.06.052
51. Payen C, Koszul R, Dujon B, Fischer G. Segmental duplications arise from Pol32-dependent repair of broken forks through two alternative replication-based mechanisms. PLoS Genet. 2008;4: e1000175. doi:10.1371/journal.pgen.1000175
52. Smith CE, Llorente B, Symington LS. Template switching during break-induced replication. Nature. 2007;447: 102–105. doi:10.1038/nature05723
53. Naseeb S, Carter Z, Minnis D, Donaldson I, Zeef L, Delneri D. Widespread Impact of Chromosomal Inversions on Gene Expression Uncovers Robustness via Phenotypic Buffering. Mol Biol Evol. 2016;33: 1679–1696. doi:10.1093/molbev/msw045
54. Colson I, Delneri D, Oliver SG. Effects of reciprocal chromosomal translocations on the fitness of Saccharomyces cerevisiae. EMBO Rep. 2004;5: 392–398. doi:10.1038/sj.embor.7400123
55. Bilanchone VW, Claypool JA, Kinsey PT, Sandmeyer SB. Positive and negative regulatory elements control expression of the yeast retrotransposon Ty3. Genetics. 1993;134: 685–700.
56. Exinger F, Lacroute F. 6-Azauracil inhibition of GTP biosynthesis in Saccharomyces cerevisiae. Curr Genet. 1992;22: 9–11.
57. Powell W, Reines D. Mutations in the second largest subunit of RNA polymerase II cause 6-azauracil sensitivity in yeast and increased transcriptional arrest in vitro. J Biol Chem. 1996;271: 6866–6873.
58. Mason PB, Struhl K. Distinction and relationship between elongation rate and processivity of RNA polymerase II in vivo. Mol Cell. 2005;17: 831–840. doi:10.1016/j.molcel.2005.02.017
59. Malagon F, Kireeva ML, Shafer BK, Lubkowska L, Kashlev M, Strathern JN. Mutations in the Saccharomyces cerevisiae RPB1 Gene Conferring Hypersensitivity to 6-Azauracil. Genetics. 2006;172: 2201–2209. doi:10.1534/genetics.105.052415
60. Martini E, Diaz RL, Hunter N, Keeney S. Crossover Homeostasis in Yeast Meiosis. Cell. 2006;126: 285–295. doi:10.1016/j.cell.2006.05.044
61. Park H, Lopez NI, Bakalinsky AT. Use of sulfite resistance in Saccharomyces cerevisiae as a dominant selectable marker. Curr Genet. 1999;36: 339–344.
62. Gietz RD, Woods RA. Transformation of yeast by lithium acetate/single-stranded carrier DNA/polyethylene glycol method. Methods Enzymol. 2002;350: 87–96.
63. Török T, Rockhold D, King AD. Use of electrophoretic karyotyping and DNA-DNA hybridization in yeast identification. Int J Food Microbiol. 1993;19: 63–80.
64. Sambrook J, Fritsch EF, Maniatis T. Molecular cloning: a laboratory manual. Cold Spring Harbor, NY, USA: Cold Spring Harbor Laboratory Press; 1989.
65. Khandjian EW. Optimized Hybridization of DNA Blotted and Fixed to Nitrocellulose and Nylon Membranes. Bio/Technology. 1987;5: 165. doi:10.1038/nbt0287-165
66. Yue J-X, Liti G. Long-read sequencing data analysis for yeasts. Nat Protoc. 2018;13: 1213–1231. doi:10.1038/nprot.2018.025

912 67. Yue J-X, Li J, Aigrain L, Hallin J, Persson K, Oliver K, et al. Contrasting evolutionary
913 genome dynamics between domesticated and wild yeasts. Nat Genet. 2017;49: 913–924.
914 doi:10.1038/ng.3847
915 68. Wagih O, Parts L. gitter: A Robust and Accurate Method for Quantification of Colony Sizes
916 from Plate Images. G3 Genes Genomes Genet. 2014; g3.113.009431. doi:10.1534/g3.113.009431
917 69. Baryshnikova A, Costanzo M, Kim Y, Ding H, Koh J, Toufighi K, et al. Quantitative analysis
918 of fitness and genetic interactions in yeast on a genome scale. Nat Methods. 2010;7: 1017–1024.
919 doi:10.1038/nmeth.1534
920